JMEPEG (2023) 32:3668–3677
https://doi.org/10.1007/s11665-022-07332-z


1059-9495/$19.00

TECHNICAL ARTICLE

# Phase Stability of AlCoTiZn High-Entropy Alloy Prepared by Mechanical Alloying

*Sushil Yebaji, Ayush Saurav, Pranjal Chauhan, B.S. Murty, Baswanta Patil, Aravindha Babu, Vaishali Poddar, and T. Shanmugasundaram*

Submitted: 18 October 2021 / Revised: 10 May 2022 / Accepted: 27 July 2022 / Published online: 16 September 2022

**In this work, synthesis and phase stability of a novel dual-phase (HCP–BCC) AlCoTiZn high-entropy alloy are presented. Microstructural evolution and thermal stability of the alloy powder were studied up to their melting point. X-ray diffraction, scanning electron microscopy, differential scanning calorimetry, atomic emission spectrophotometry analysis and hardness measurements were used for the characterization of the HEA. As-milled and the bulk samples consist of an HCP and Co-rich BCC dual phases. The samples heat-treated at intermediate temperatures show HCP and Co-rich two FCC phases. Thermal stability studies reveal that vaporization of Zn occurs at around 800 °C. An extraordinary hardness of 1005 ± 50 HV was observed in the bulk sample. This is mainly attributed to the presence of dual-phase HCP–BCC structures.**

**Keywords** hexagonal close-packed structure, high-entropy alloys, mechanical alloying, phase stability

## 1. Introduction

High-entropy alloys (HEAs) have received more attention in recent times due to their remarkable properties. These alloys consist of multiple components with stoichiometric composition lying between 5 and 35% (Ref 1). It has been reported that HEAs with stable single or multiphase microstructures shows extraordinary properties such as wear resistance, corrosion resistance, room and high-temperature strength (Ref 2-7). Phase formation and stability of the phases are predicted using different thermodynamic parameters such as atomic size mismatch ($\delta$), enthalpy of mixing ($\Delta H_{mix}$), mixing entropy ($\Delta S_{mix}$), $\Omega$ and valence electron concentration (VEC) (Ref 8-11). Among these, VEC is used to predict the phases present in the systems. For example, face-centered cubic (FCC) structure has been observed when VEC of alloy exceeds 8. Body-centered cubic (BCC) structure is observed when the VEC value drops below 6.8. In between these two values, dual-phase (FCC and BCC) structure is mainly observed (Ref 2, 10, 12-18). Very recently, HEAs with a hexagonal close-packed (HCP) structure have been reported (Ref 14, 19-22). Recent studies show that VEC value for HCP-based HEAs is less 3 (Ref 23).

Various Zn containing high-entropy alloys have been processed via mechanical alloying (Ref 24-31). AlFeTiCrZnCu alloy had thermal stability up to 800 °C and exhibit high hardness and high wear resistance (Ref 25). CuNiCoZnAl alloy had ordered phase of FCC-L12 (Ref 30). AlCrCuFeZn combination had majorly BCC structure after mechanical alloying while FCC–BCC composite had been cited after compaction (Ref 27). The major phases observed in these alloys were FCC and BCC (Ref 25, 27, 30, 32). AlCrCuFeZn manufactured with mechanical alloying followed by spark plasma sintering (SPS) had two phased body-centered cubic (BCC) with 91% density. Sintered sample had dual-phase structure with CuZn- and FeAlCr-rich BCC phases with hardness up to 627 HV (Ref 31).

It has been reported that systems with Zn such as $Ti_{20}Fe_{20}Cr_{20}Cu_xZn_y$ and AlCoCrCuFeMoNiTiVx ($x$ = Mn, Zn) show excellent hardness (Ref 18-20, 32). The first HEAs such as BeCoMgTi and BeCoMgTiZn with HCP crystal structure were synthesized by mechanical alloying using the principal elements having HCP crystal structure in equimolar compositions. However, these alloys had an amorphous structure due to huge lattice distortion (Ref 33). It has been reported that the use of rare earth metals (as majority of the elements exhibit HCP structure) leads to the formation of single-phase HCP crystal structure (Ref 34). A similar trend has been noticed during the fabrication of HEAs with Y/La series elements showing a single-phase HCP structure in equimolar concentrations of HoDyYGdTb (Ref 35). Very recently, single-phase HCP was observed in the annealing of FCC lightweight $Al_{20}Li_{20}Mg_{10}Sc_{20}Ti_{30}$ high-entropy alloy, and it was found that the hardness of the alloy after annealing (HCP phase) is better than the initial state (FCC phase) (Ref 35, 36). The literature clearly shows that only a few HCP-based high-entropy alloys using rare earth elements (HCP metals) have been developed till now. Therefore, in this work, we try to develop HCP HEAs using 3-d transition metals such as Zn, Co and Ti. Further, it was found that the addition of minor amount FCC elements can help to retain HCP phase (Ref 2, 3). Therefore, in this work AlTiZnCo HEA alloy system is designed based on thermodynamic parameters (Table 1). Most of the HCP-based HEA system were developed through mechanical alloying and were observed only in as-milled state. Nevertheless, most practical

**Sushil Yebaji, Ayush Saurav, Pranjal Chauhan,** and **T. Shanmugasundaram**, Department of Metallurgical and Materials Engineering, Defence Institute of Advanced Technology, Pune, India; **B.S. Murty**, Indian Institute of Technology Hyderabad, Hyderabad, India; **Baswanta Patil**, International Advanced Research Centre for Powder Metallurgy, Hyderabad, India; **Aravindha Babu**, Defence Metallurgical Research Laboratory, Hyderabad, India; **Vaishali Poddar**, College of Engineering Pune, Pune, India. Contact e-mails: ss.thangaraju@gmail.com and thangaraju@diat.ac.in.

**Table 1 Calculated thermodynamic parameters for AlCoTiZn**

| Alloy composition | $\Delta H_{mix}$, kJ mol$^{-1}$ | $\Delta S_{mix}$, J mol$^{-1}$ K$^{-1}$ | $\delta$, % | $\Omega$ | VEC |
|---|---|---|---|---|---|
| AlCoTiZn | −24 | 11.526 | 5.83 | 0.64 | 7 |

applications require the alloys in a bulk and stable form. Most consolidation techniques require the powders to be heated to high temperature. Therefore, the thermal stability study of any mechanically alloyed system is of paramount importance. However, the thermal stability of HCP-based HEAs has been least explored.

In this work, a novel AlTiCoZn dual-phase HCP–BCC-based high-entropy alloy is synthesized through mechanical alloying. Also, thermal stability and microstructural evolution are studied up to the melting temperature. The present study provides an insight into the phase stability of dual-phase HEAs containing volatile elements such as zinc.

## 2. Materials and Methods

Elemental powders of Al, Ti, Co and Zn (from Alfa Aesar, USA) of purity greater than 99.5% were used as a starting material. The elemental powders were milled in a planetary ball mill (Pulverisette-5, Frisch) with WC vials and balls (diameter = 0.01 m). The powders were milled at 300 rotations per minute and 10:1 ball-to-powder ratio. The alloying was carried out in a wet milling condition where toluene was used as a process control agent. The milling was interrupted every 30 min with a pause time of 10 min to prevent the heating of powders. Powder samples were collected for characterization at 5, 10, 20 and 30 h of milling.

Differential scanning calorimetric (DSC) measurements were taken using a STA 449 Fe Jupiter DSC. As-milled powder samples were heated in an alumina pan up to 1400 °C and cooled at a rate of 10 °C/min; procedure had been repeated on heat-treated sample without removing sample from alumina pan for second run. Green compacts of 10 mm diameter and 5 mm height were prepared from 30 h ball-milled powder using a hydraulic press. Based on the DSC results, the green compacts were heat-treated/sintered in a vacuum ($10^{-4}$ Torr) at various temperatures, 800, 900, 1100, 1300 and 1400 °C with a very slow heating rate (1 °C/min), and all the samples were held for 5 min. The sample heat-treated till the melting point (1400 °C) is referred as bulk sample. X-ray diffraction (XRD) analysis was carried out on as-ball-milled and heat-treated samples using a Bruker D8 FOCUS diffractometer with V-filtered Cu K$\alpha$ ($\lambda$ = 1.54 Å) radiation. A scanning electron microscope (SEM) (ZEISS SEM FEI) equipped with energy-dispersive spectroscopy (EDS) (Inca PENTA FET X3, Oxford Instruments) was used to analyze the microstructure and chemical composition of the samples. XRD analysis of the samples was carried out by matching the diffraction patterns with the available data base using a X'Pert High Score Plus software. In addition, analysis of HCP phase was also carried out manually using the Eq. 1. Initially, 'a' and 'c' values obtained from (100) and (002) reflections and then '*d*' values for all the reflections were obtained using the Eq. 1. The '*d*' values obtained from the calculation and the experiments are given in Table 3.

$$d = \left(\frac{4}{3}\left(\frac{h^2 + hk + k^2}{a^2}\right) + \frac{l^2}{c^2}\right)^{-1/2} \quad \text{(Eq 1)}$$

A micro-plasma atomic emission spectrometer (MP-AES, Agilent technology, USA, 4200, G8003A) was used to identify the composition of the heat-treated samples. The sample for MP-AES measurement was prepared with 200 times dilution of heat-treated powders in aqua regia. Hardness of the samples was obtained using a Vickers micro-hardness tester (Matzuzawa Nxt 7). The applied load was 500 gmf with a dwell time of 10 s. The average hardness was obtained from ten measurements at different points on the sample.

## 3. Results

### 3.1 Mechanical Alloying of AlCoTiZn HEA

Various thermodynamic parameters have been proposed to predict phase stability in HEAs (Ref 18, 20, 23, 32-35, 37). The design of alloy was done through thermodynamic parameters such as atomic size mismatch ($\delta$), enthalpy of mixing ($\Delta H_{mix}$), mixing entropy ($\Delta S_{mix}$), $\Omega$, and valence electron concentration (VEC).

The atomic size mismatch ($\delta$) is used to estimate the amount of lattice strain present in the alloy (Ref 23), given by Eq. 2

$$\delta = 100\sqrt{\sum_{i=1}^{n} x_i\left(1 - \left(r_i / \sum_{i=1}^{n} x_i r_i\right)\right)^2} \quad \text{(Eq 2)}$$

where $x_i$ and $r_i$ are the atomic percentage and atomic radius of the $i$th element.

The enthalpy of mixing ($\Delta H_{mix}$) is defined by Eq. 3,

$$\Delta H_{mix} = \sum_{i=1, i\neq j}^{n} 4\Delta H_{i-j}^{mix} x_i x_j \quad \text{(Eq 3)}$$

where $\Delta H_{i-j}^{mix}$ is the enthalpy of mixing between the $i$th and $j$th elements; and $x_i$ and $x_j$ are the atomic ratios of the $i$th and $j$th components, respectively (Ref 38).

The amount of change in mixing entropy is calculated using Eq. 4,

$$\Delta S_{mix} = -R\sum_{i=1}^{n} x_i \ln x_i \quad \text{(Eq 4)}$$

where $R$ is the gas constant (8.314 J/K mol)(Ref 38).

The dimensionless stability parameter '$\Omega$' can be estimated using Eq. 5,

$$\Omega = \Delta S_{mix}\left(\sum_{i=1}^{n} x_i (T_m)_i\right) \Big/ |\Delta H_{mix}| \quad \text{(Eq 5)}$$

where $(T_m)_i$ is the melting temperature of the $i$th element of the alloy. The value of $\Omega$ is proposed to be greater than 1 for the formation of a stable solid solution (Ref 39).

The valence electron concentration (VEC) is used to determine the phase and obtained by Eq. 6

$$\mathrm{VEC} = \sum_{i=1}^{n} x_i (\mathrm{VEC})_i \quad \text{(Eq 6)}$$

where $(\mathrm{VEC})_i$ is the VEC of the $i$th element (Ref 37).

The calculated values of the above-mentioned thermodynamic parameters for the AlCoTiZn alloy are given in Table 1. The proposed VEC value for a HEA to form a BCC structure is ≤ 6.67; for the FCC structure, VEC ≥ 8. A mixed microstructure is supposed to form between 6.67 and 8 (Ref 37). However, there is not any commonly accepted VEC value/range for HCP structure. It has been recently reported that VEC for HCP structure falls below 3 (VEC ≤ 3) (Ref 23). However, further experimentation/database would be required to substantiate this claim as the literature for HCP-based HEAs is scant. Atomic radius, VEC, melting temperature and mixing enthalpies of atomic pairs of Al, Co, Ti and Zn are provided in Table 2.

The value of $\Delta H_{\mathrm{mix}}$ and $\delta$ is within the range of solid solution formation. Since the system contains four elements, $\Delta S_{\mathrm{mix}}$ is slightly less. According to Eq. 4, $\Omega$ is directly related to $\Delta S_{\mathrm{mix}}$ and if $\Omega$ becomes less than 1.1 as in this composition, it will satisfy one of the favorable conditions for amorphous phase formation. Also, the VEC value of 7 indicates that the structure could be FCC and BCC as per the VEC criteria. However, the XRD analysis of the sample as shown in Fig. 1 shows crystalline phase mix formation of HCP and BCC. Therefore, the $\Omega$ value or the VEC criterion is insufficient to predict the phase formation in HEA, especially for HCP, which is in tune with recent studies (Ref 37).

Figure 1(a) shows the XRD patterns of mechanically alloyed powder of AlCoTiZn at 5, 10, 20, 30 h and pre-milled powder, and Fig. 1(b) shows the XRD pattern of 30 h sample with intensity in logarithmic scale. The diffraction peaks of individual elements can be observed in pre-milled conditions (0 h). A change in the initial peaks is observed after 5 h of milling, confirming the initiation of alloy formation. The XRD patterns 20 and 30 h of milling are nearly identical. However, milling is carried out for up to 30 h for a complete dissolution of alloying elements and alloy formation. The analysis of the milled powder shows that the peaks have no similarity with the well-established database of various Al-, Co-, Ti- and Zn-based alloy systems, which ensure the complete dissolution of all the allotting elements. The 30 h ball-milled powder contains HCP and BCC phases. The '$d$' values obtained from the calculation and the experiments are given in Table 3. The lattice parameters of the HCP phase are found to be $a$ = 2.84 Å and $c$ = 4.95 Å.

The lattice parameter of the BCC phase was 2.87 Å. The volume fraction of the HCP and BCC phase in 30 h ball-milled powder was 58 and 42%, respectively.

Elemental maps and BSE image of 30 h milled AlCoTiZn alloy powder is shown in Fig. 2. Ti is dispersed throughout the alloy matrix. A close examination of the figure shows some Al deficit areas in the microstructure (shown by yellow arrows). The EDS compositional analysis reveals that the marked regions are deficit in Al and rich in Ti with Co and Zn.

**Table 2 Atomic radius, VEC, melting temperature and mixing enthalpies of atomic pairs present in AlCoTiZn**

| Element | Al | Co | Ti | Zn |
|---|---|---|---|---|
| Radius, in pm | 143.17 | 125.10 | 146.15 | 139.45 |
| VEC | 3 | 9 | 4 | 12 |
| Melting temperature, in K | 933 | 1768 | 1941 | 692.53 |
| Mixing enthalpies $\Delta H_{i-j}^{\mathrm{mix}}$, kJ/mol | | | | |
| Co | − 19 | … | … | … |
| Ti | − 30 | − 28 | … | … |
| Zn | 1 | − 5 | − 15 | … |

### 3.2 Phase Stability Study AlCoTiZn HEA

Figure 3 shows the DSC curve of 30 h mechanically alloyed (MAed) AlCoTiZn powder. During the first run, three significant endothermic peaks are observed at around 800, 905 and 1333, with one mild exothermic peak at 500 °C and one significant at 1100 °C. The DSC second heating cycle shows only one endothermic peak at 1333 °C, which is related to the melting of the AlCoTiZn alloy, and it also indicates that there is no phase transformation till its melting point. The second run of the DSC was carried out on the same sample without removing it from the machine after the first run. The presence of only one endothermic peak (melting) during the second run of the DSC indicates that the alloy is in more stable state after the melting (during first run). The first exothermic peak (500 °C) implies the formation of new phases (FCC) in the system, while the second endothermic peak observed at 800 °C could be attributed to vaporization of Zn. Later, the atomic emission spectrophotometry (AES) analysis of heat-treated samples was studied to quantify the Zn vaporization from the alloy. The chemical composition of as-milled and annealed AlCoTiZn powders obtained by AES analysis is shown in Table 4. Evaporation of Zn is started occurring from 700 °C, and complete evaporation is occurred at around 800 °C. The second endothermic peak observed at around 900 °C could be related to dissolution of the phase that formed at 500 °C. EDS analyses of the heat-treated samples also show only a trace of Zn (less than 0.5%) after 800 °C (Table 4). Other elements, namely Al, Co and Ti, appear to be stable up to the near melting point of the alloy. The atomic fraction of Al, Co and Ti remains constant at 21, 40 and 38%, respectively, up to 1300 °C, followed by a minor change at 1400 °C. An exothermic peak at 1100 °C suggests a new phase transformation (Also see Table 5). The sharp endothermic peak at 1333 °C is the melting temperature of AlCoTiZn alloy.

Figure 4 shows the XRD pattern of the heat-treated samples at a temperature of 800, 900, 1100 and 1300 °C. The XRD patterns of heat-treated samples show a few additional peaks compared to that of as-milled powders, thus indicating the formation of new phases. These new phases could have formed at around 500 °C (Fig. 3, a broad exothermic peak at 500 °C). Rietveld analysis of XRD data was performed for all the conditions for quantitative analysis using a X'Pert High Score Plus software. The parameter derived from the XRD analysis of heat-treated powders is presented in Table 5. The alloy displays a dynamic change in phase fraction with respect to temperature. The XRD analysis of samples at higher temperatures reveals that annealing of the sample results in the formation of two FCC phases (FCC1 and FCC2) and an HCP phase. The phase transformation from parent BCC + HCP to FCC1 + FCC2 +

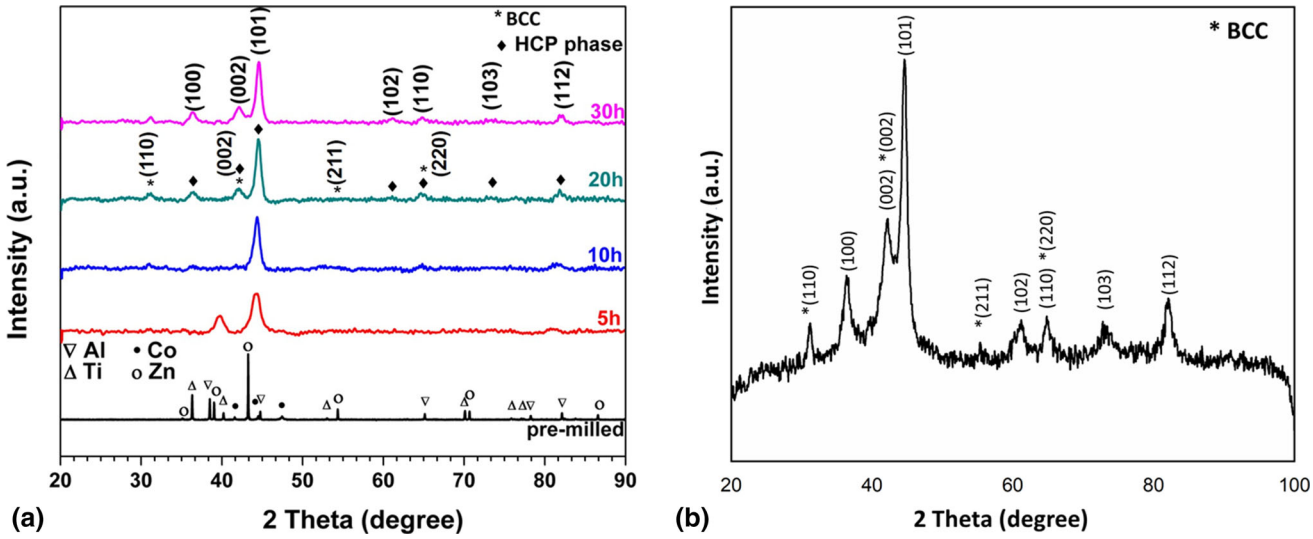


**Fig. 1** (a) X-ray diffraction patterns of AlCoTiZn alloy at different milling times. (b) XRD pattern of 30 h sample with intensity in logarithmic scale

**Table 3 HCP phase calculation**

| | | | | | | | | *a* | *c* | *c*/*a* | |
|---|---|---|---|---|---|---|---|---|---|---|---|
| | | | | | | | **1** | **2.85** | **4.28** | **1.50** | |
| | | | | | | | | **Calculation factors** | | | |
| **2theta** | **theta** | **Sin (theta)** | ***d* spacing** | $d^2$ | ***h*** | ***k*** | **l** | ***a*** | ***c*** | **Calculated '*d*'** | **Percentage deviation** |
| 36.41 | 0.32 | 0.31 | 2.46 | 6.07 | 1.00 | 0.00 | 0.00 | 2.85 | 0.00 | 2.46 | 0.00 |
| 42.17 | 0.37 | 0.36 | 2.14 | 4.58 | 0.00 | 0.00 | 2.00 | 0.00 | 4.28 | 2.14 | 0.00 |
| 44.55 | 0.39 | 0.38 | 2.03 | 4.13 | 1.00 | 0.00 | 1.00 | 2.35 | 2.03 | 2.14 | 5.15 |
| 61.03 | 0.53 | 0.51 | 1.52 | 2.30 | 1.00 | 0.00 | 2.00 | 1.75 | 3.03 | 1.62 | 6.57 |
| 64.81 | 0.57 | 0.54 | 1.44 | 2.06 | 1.00 | 1.00 | 0.00 | 2.87 | 0.00 | 1.42 | − 0.97 |
| 73.21 | 0.64 | 0.60 | 1.29 | 1.67 | 1.00 | 0.00 | 3.00 | 1.49 | 3.87 | 1.23 | − 4.37 |
| 80.01 | 0.70 | 0.64 | 1.20 | 1.43 | 1.00 | 1.00 | 2.00 | 2.40 | 2.40 | 1.18 | − 1.07 |
| 80.01 | 0.70 | 0.64 | 1.20 | 1.43 | 1.00 | 1.00 | 2.00 | 2.40 | 2.40 | 1.18 | − 1.07 |

HCP may have taken place at 500 °C as indicated by the exothermic peak at 500 °C. In detail, the phases present at intermediate temperatures ( ≥ 500 °C) consist of two Al-Ti-Co-rich FCC (space group: Fm-3m 225) and Al-Ti-rich HCP phases (space group: P 63/m m c). One of the FCC phases (FCC1) has a lattice parameter of approx. 5.80 Å, whereas the other FCC phase (FCC2) has a lattice parameter of 11.87 Å. The lattice parameters of the two FCC phases remained approximately constant at all temperatures. The major change was observed at 900 °C, where the c/a ratio of the HCP phase changed drastically from 2.19 to 1.77. A continuous reduction in c/a ratio of HCP was observed with an increase in temperature. Also, the phase fraction of the HCP phase remained nearly constant till 1100 °C. However, a drastic increase in the weight fraction of HCP (from 18 to 41%) was observed at 1300 °C.

Figure 5 shows the SEM image of the alloy powders heat-treated at various temperatures. The distribution of the phases can be clearly observed. The XRD analysis (Via Rietveld refinement) suggests that the BCC phase is rich in Co, whereas the HCP phase is rich in Al and Ti. The phases were indexed as BCC or HCP based on XRD analysis (Rietveld refinement) and x-ray spectroscopy (EDS) analysis. The EDS analysis was used to analyze the composition of each region in the micrograph. Figure 6 shows the variation of Co and Al at various heat treatment conditions. The Rietveld analysis (Via Wyckoff position refinement) of the heat-treated samples revealed that FCC phase is rich in Al, Co and Ti while HCP is rich in Al and Ti. It was also found that (Table 4) FCC is the major phase in the alloy at all intermediate temperatures. Also, two different phase contrasts are clearly visible in the SEM images of the alloy (Fig. 5). Based on the EDS analysis, it can be clearly seen that the dark phase is deficient in Co (and rich in Al) and the bright phase is rich in Co. The combined EDS and XRD analysis were used to designate the bright phase as BCC (only in as-milled and bulk sample) and FCC (heat-treated samples) and the dark phase as HCP (presence in all the conditions). The variation of Al and Co content in various phase is already given in Fig. 6 of the manuscript. The sample was slowly heated to 1400 °C to better understand AlCoTiZn alloy behavior near its melting point. The microstructural characterization and hardness of the post-melted consolidated bulk sample were studied. Figure 7 shows the XRD patterns of 30 h as-milled and post-melted samples of AlCoTiZn.

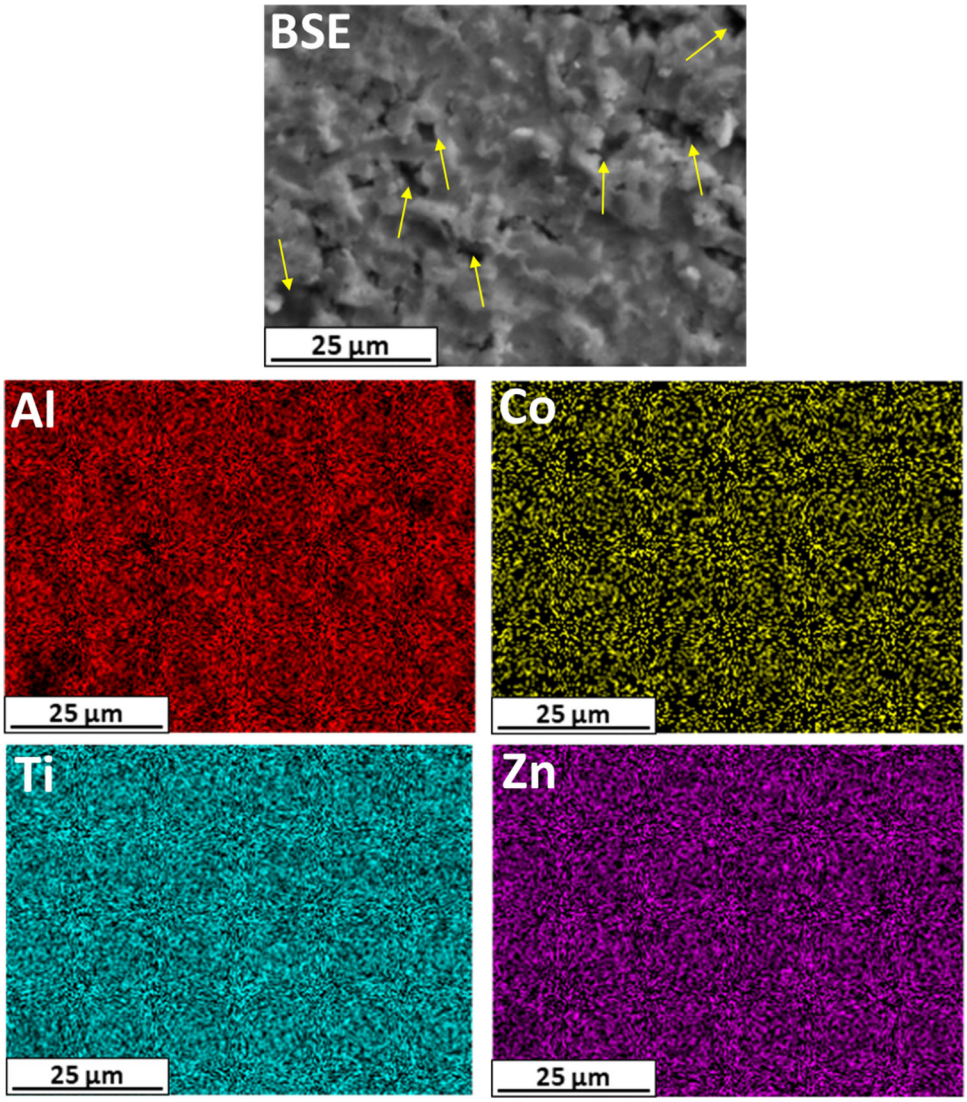


**Fig. 2** SEM (BSE) and elemental mapping image of 30 h milled AlCoTiZn alloy powder. The yellow arrows point to Al deficient areas (Color figure online)

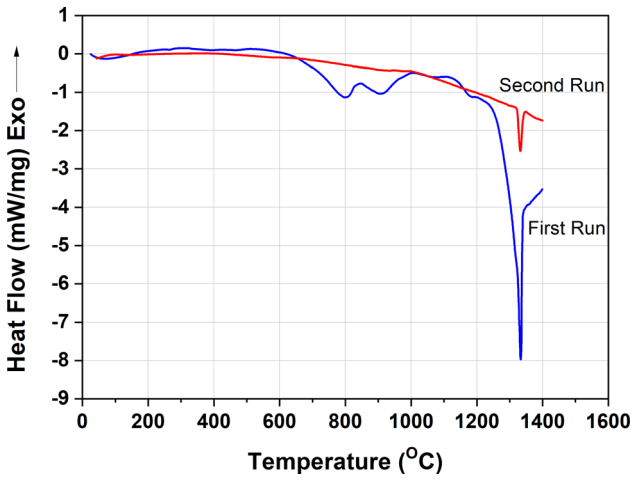


**Fig. 3** DSC of 30 h mechanically alloyed AlCoTiZn powder

**Table 4 Chemical composition (at.%) of as-milled and annealed AlCoTiZn powder**

| Elements\conditions | %Al | %Co | %Ti | %Zn |
|---|---|---|---|---|
| As-milled | 15.51 | 31.95 | 24.49 | 28.05 |
| At $T$ = 800 °C | 20.97 | 40.31 | 37.14 | 01.59 |
| At $T$ = 900 °C | 20.87 | 40.39 | 38.43 | < 0.5 |
| At $T$ = 1100 °C | 20.66 | 40.88 | 38.45 | < 0.5 |
| At $T$ = 1300 °C | 20.55 | 40.86 | 38.58 | < 0.5 |
| At $T$ = 1400 °C | 17.79 | 55.72 | 26.25 | < 0.5 |

The XRD pattern obtained from the post-melted sample at 1400 °C was like the XRD pattern of the as-milled sample. The XRD peaks of post-melted were sharp in contrast to the peaks of as-milled samples. Again, the XRD analysis of the post-melted sample suggests that it contains two phases. One of the phases was identified as BCC (Pm-3 m 221), and the other phase was identified as the HCP phase, like as-milled 30 h powder. The

**Table 5 XRD analysis of heat-treated powders**

| Sr. No. | Temperature | Phase | Lattice parameter, Å | | Weight fraction, % |
|---|---|---|---|---|---|
| 1 | As-milled | BCC (BCC1) | $a$ = 2.87 | | 42 |
| | | HCP | $a$ = 2.85 | $c$ = 4.28 | 58 |
| | | | $c/a$ = 1.50 | | |
| 2 | 800 °C | FCC (FCC1) | $a$ = 5.80 | | 52 |
| | | FCC (FCC2) | $a$ = 11.87 | | 28 |
| | | HCP | $a$ = 2.67 | $c$ = 5.84 | 20 |
| | | | $c/a$ = 2.19 | | |
| 3 | 900 °C | FCC (FCC1) | $a$ = 5.81 | | 50 |
| | | FCC (FCC2) | $a$ = 11.87 | | 30 |
| | | HCP | $a$ = 2.67 | $c$ = 4.56 | 20 |
| | | | $c/a$ = 1.77 | | |
| 4 | 1100 °C | FCC (FCC1) | $a$ = 5.80 | | 46 |
| | | FCC (FCC2) | $a$ = 11.84 | | 35 |
| | | HCP | $a$ = 2.83 | $c$ = 4.55 | 19 |
| | | | $c/a$ = 1.61 | | |
| 5 | 1300 °C | FCC (FCC1) | $a$ = 5.84 | | 34 |
| | | FCC (FCC2) | $a$ = 11.88 | | 25 |
| | | HCP | $a$ = 2.88 | $c$ = 4.60 | 41 |
| | | | $c/a$ = 1.60 | | |
| 6 | 1400 °C | BCC (BCC1) | $a$ = 2.86 | | 55 |
| | | HCP | $a$ = 2.92 | $c$ = 4.66 | 45 |
| | | | $c/a$ = 1.59 | | |

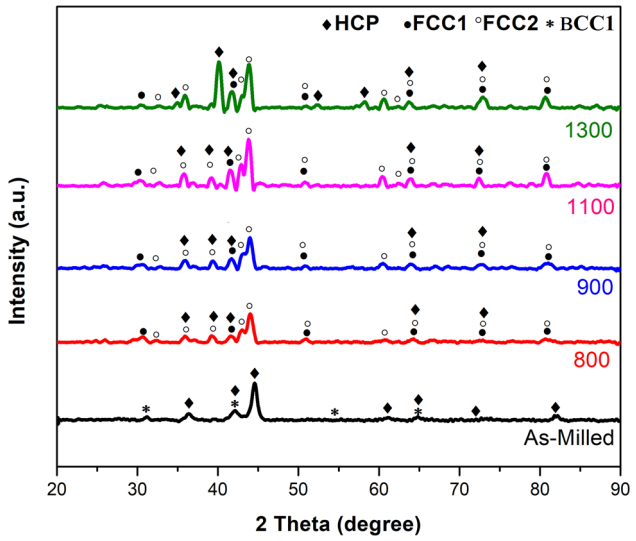


**Fig. 4** X-ray diffraction patterns of as-milled and heat-treated (800, 900, 1100 and 1300 °C) AlCoTiZn alloy

lattice parameters of the HCP structure are 2.85 and 4.28 Å, respectively, with an axial ratio of 1.50 (close to the axial ratio of the HCP structure (1.63)). The BCC phase has a lattice parameter of 2.86 Å. The BSE image and the corresponding elemental mapping of the post-melted sample are shown in Fig. 8. The two distinct phases are visible in the image with different compositions. One of the phases (identified as BCC) is rich in Co, and the other phase (HCP) is rich in Ti. Again, both EDAX and XRD (Rietveld analysis) were used to index the phases. No traces of Zn were visible in SEM analysis of the post-melted samples.

The post-melted AlCoTiZn sample had a hardness of 1005 ± 50 HV. The presence of intermetallic phases and HCP structure could be the reason for such extraordinary hardness and brittleness.

## 4. Discussion

The present study aims at developing a novel HCP-based HEA and studying the phase stability of the same. However, the apparent difficulty in designing an HCP-based HEA is the lack of sufficient data, which results in a poor understanding of phase formation and stability criteria. Nonetheless, the AlCoTiZn alloy composition was designed in this study. The thermodynamic parameters of the alloy are given in Table 1 and 2. The $\Delta S_{mix}$ of the alloy is 11.56 J mol$^{-1}$ K$^{-1}$. Although the alloy does not satisfy the component-based definition of HEA, it can be classified as HEA through entropy-based definition. The enthalpy of mixing of the alloy ($\Delta H_{mix}$) is -24 kJ mol$^{-1}$. Such a high negative value of $\Delta H_{mix}$ often promotes intermetallic phases in a HEA. Also, the $\Delta H_{mix}$ of most element combinations/pairs (Table 2) is highly negative, suggesting a high possibility of forming multiple binary intermetallics. It has been previously reported that a high value of $\Omega$ ( $\geq$ 1.1) and a small value of $\delta(\leq 6.6\%)$ promote the formation of high-entropy stabilized solid solution phase (Ref 23). The $\Omega$ of the alloy considered in this study is 0.64, which is significantly less than 1.1. The VEC of the alloy is 7. The VEC rule suggests that the alloy should be dual-phase FCC–BCC. Surprisingly, the alloy is a simple dual-phase HCP–BCC as opposed to multiple complex intermetallic phases. The VEC rule is one of the most accepted criteria for phase prediction in HEAs. However, many exceptions to the VEC rule have already been reported (Ref 37). Also, the absence of multiple complex intermetallic phases (expected due to high negative values of $\Delta H_{mix}$) implies that entropy was able to stabilize simple solid solution phase even with low $\Omega$. The above observations suggest that the current conventions/rules for HCP-based high entropy are insufficient for phase prediction and stability and warrant further investigation.

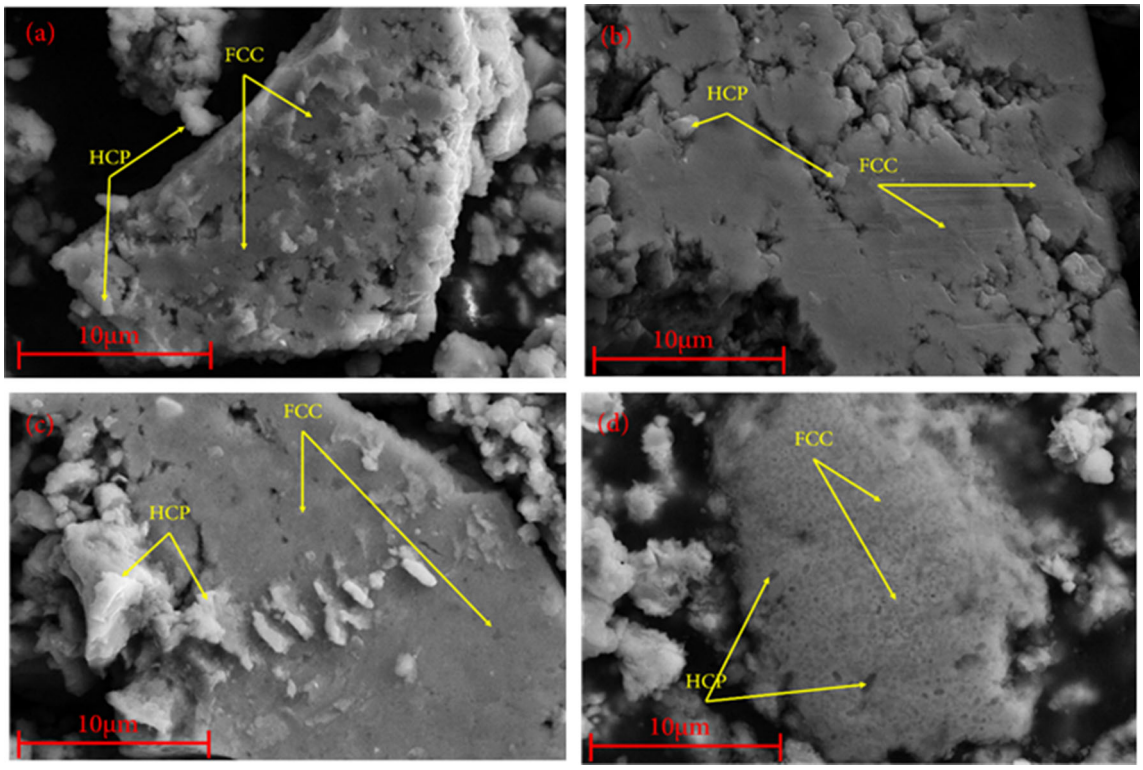


**Fig. 5** SEM micrograph of individual powder particles heat-treated at (a) 800 °C, (b) 900 °C, (c) 1100 °C and (d) 1300 °C

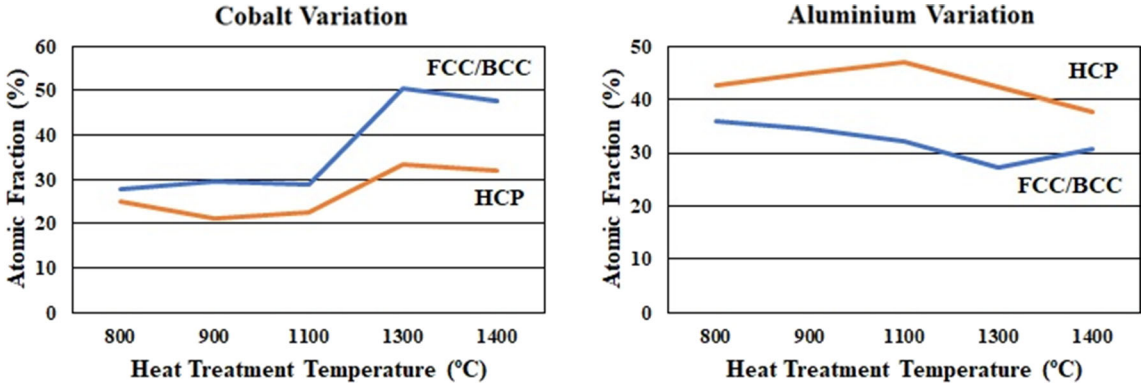


**Fig. 6** Variation of Co and Al at various heat treatment temperatures

In this work, mechanical alloying was preferred over melting and solidification (such as vacuum arc melting (VAM)) due to the presence of Zn in the system which evaporates at around 900 °C (Ref 40), thus making it unsuitable to be synthesized by VAM. The XRD analysis and DSC analysis (Table 5) suggest that BCC to FCC (FCC1 + FCC2) may have occurred at 500 °C. The thermal stability study reveals the metastable nature of the 30 h mechanical alloyed powder. Evaporation of Zn started at 700 °C and completed nearly at 800 °C. EDS analyses (Table 4) of the heat-treated sample (800 °C) also show only traces of Zn (less than 0.5%). The XRD analysis of the 30 h MAed samples shows no trace of any individual element (Fig. 1). One of the hypotheses during the design of this alloy was that the Zn melting/evaporation could be avoided with alloying, and as Zn forms of the solid solution, individual property of the Zn (such as melting point) would have no significance. However, the current result suggests that the volatile element, such as Zn, may evaporate from the alloy. This raises a conceptual conundrum regarding such alloys to be defined as high-entropy alloys. Clearly, as the Zn has evaporated out of the system at higher temperatures, the alloy now only has 3 elements. The three-component alloys cannot be defined as HEA by any of the definitions. However, such questions are tricky to answer. A similar dilemma is experienced when the HEAs contain binary complex intermetallic phases such as NiAl, TiAl. Such phases should not be considered as HEA as they are based on two components only. However, many studies have considered such alloys (containing binary intermetallic phases) as high-entropy alloys. Such classification is derived from the assumption that the alloy has a single value of entropy (configurational entropy). However, the entropy can change with temperature. Also, complete solubility of all the alloying elements across all the composition range and temperature is seldom observed. In

reality, the chemical partition between the parent and product phases at first-order transformation is common for most HEAs. In our view, it would be better to call such alloys multiprincipal element alloys (MPEAs) as compared to HEAs.

However, a constant decrease in c/a ratio of the HCP phase was observed up to the alloy's melting point (Table 5). The change in c/a ratio is drastic (decreases from 2.19 to 1.61) in the range of 800-1100 °C followed by gradual/very minute (1.61 to 1.59) change after 1100 °C. This suggests that the change in c/a ratio of HCP phase may be caused by the evaporation of the residual Zn that might be present in the system till 1100 °C. The lattice parameter of the two FCC phases remained practically constant across the temperature range. However, a different trend is observed in the change of the wt.% of the phases. The wt.% of the FCC and HCP phases remained nearly constant in the temperature range of 800-1100 °C only to cause significant change at 1300 °C (Table 5). The change is again observed post-melting. The above observation suggests that phase formation and stability in this alloy are not sensitive to Zn content and depend strongly on temperature. This is also substantiated by the fact that phases formed in as-milled (containing Zn) and post-melt (without Zn) are almost the same (Fig. 7). The only difference is the c/a ratio of the HCP phase, which was 1.81 in as-milled sample compared to 1.59 in post-melted samples. Again, the difference in c/a ratio might be due to the absence of zinc in the post-melted sample.

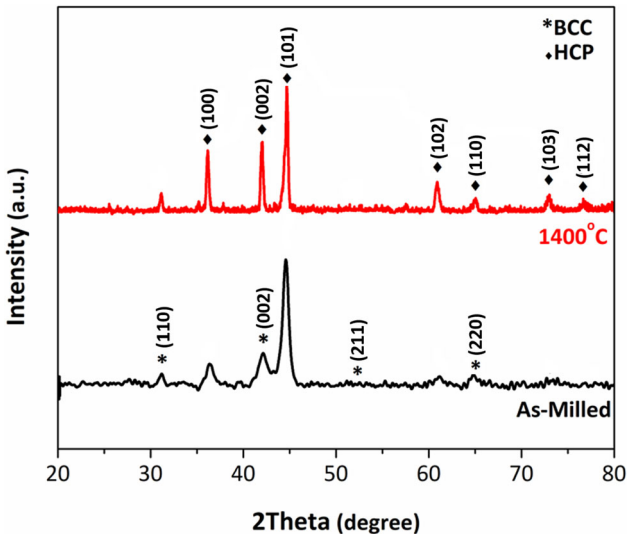


**Fig. 7** X-ray pattern of as 30 h as-milled powder and a consolidated bulk sample of AlCoTiZn

The post-melted samples contain a Co-rich BCC and a Ti-rich HCP phase. The wt. fraction of the BCC and HCP phases was found to be 55 and 45%, respectively. The presence of a dual-phase BCC–HCP structure resulted in an extraordinary hardness of 1005 ± 50 HV with density around 5.47 g cm$^{-3}$. Such a high harness is expected to impart a brittle nature in the alloy. The brittle nature of the alloy is evident from the cracks generated during the hardness testing of the alloy. For the comparison, the hardness of the current system is compared with that of other reported HEA systems with density lesser than 7 g cm$^{-3}$. Table 6 shows the density, hardness and density ratio of various HEAs. It is evident that AlCoTiZn alloy shows

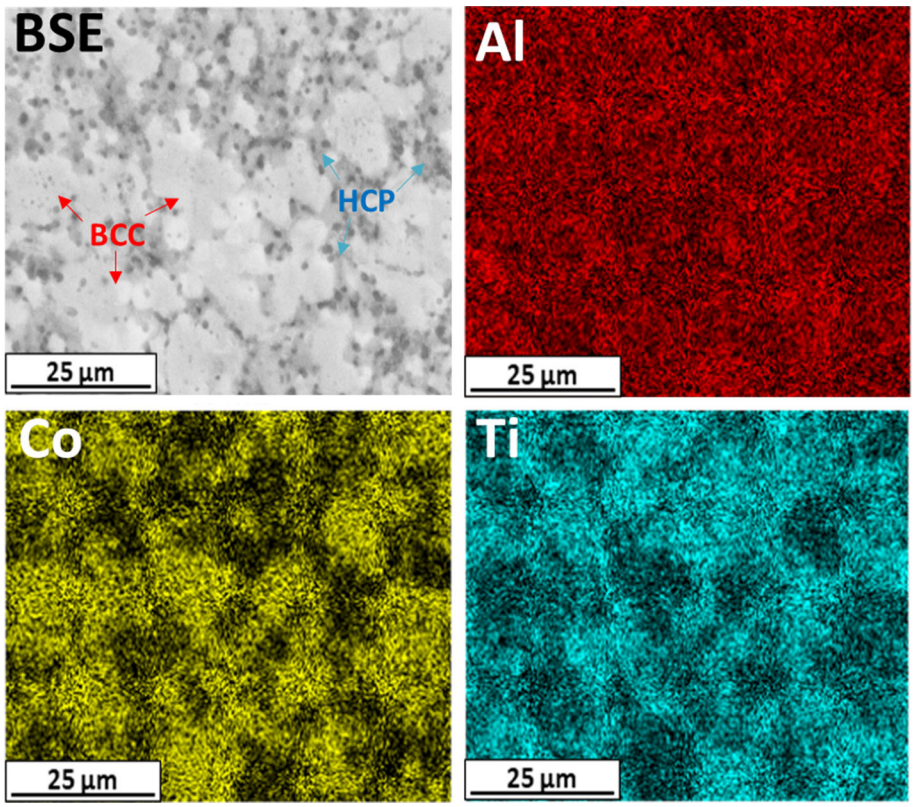


**Fig. 8** SEM (BSE) image of post-melted AlCoTiZn alloy

**Table 6 Comparison of the density, hardness and hardness-to-density ratio of AlCoTiZn alloy with other HEAs**

| Alloys | Phase | Theoretical density, g $cm^{-3}$ | Hardness, HV | Hardness/density, HV $cm^3$ $g^{-1}$ | References |
|---|---|---|---|---|---|
| AlCoTiZn | HCP + BCC | 5.47 | 1005 | 184 | This work |
| $Al_{20}Li_{20}Mg_{10}Sc_{20}Ti_{30}$ | HCP | 2.67 | 601.6 | 225 | Ref 36 |
| AlCuNiTi | FCC | 5.7 | 537 | 94 | Ref 41 |
| AlCoCrFeNi | BCC | 6.7 | 520 | 78 | Ref 42 |
| $Al_3CoCrFeNi$ | BCC | 5.3 | 506 | 95 | Ref 43 |
| CrNbTiVZr | BCC + Im | 6.6 | 482 | 73 | Ref 44 |
| AlCoCuFeNi | FCC + BCC | 7 | 536 | 77 | Ref 45 |
| AlCoCuFeNiZr | FCC + BCC + Im | 6.9 | 472 | 68 | Ref 45 |
| AlCrCuFeZn | BCC + Im | 5.9 | 627 | 106 | Ref 31 |

Im stands for intermetallic phase

better relative hardness than many other HEAs. The hardness-to-weight ratio of lightweight HCP ($Al_{20}Li_{20}Mg_{10}Sc_{20}Ti_{30}$) HEA is slightly better than the AlCoTiZn system. In conclusion, mechanical alloying and thermal stability studies clearly show that AlCoTiZn alloy has a two-phase microstructure with excellent hardness-to-weight ratio.

## 5. Conclusions

A novel AlCoTiZn high-entropy alloy was synthesized by high-energy ball milling followed by sintering. Green compacts of 30 h mechanically alloyed powders were heat-treated at different temperatures up to its melting point to study the phase stability and microstructural evolution. The mechanically alloyed 30 h powder and bulk samples (post-melted) have a dual-phase HCP–BCC structure. The melting point of AlCoTiZn alloy was found to be 1333 °C. Phase evolution, DSC analysis and thermal stability study indicate evaporation of Zn and phase transformation at intermediate temperature. The intermediate phases consist of two FCC phases and an HCP phase. The phase analysis in this study suggests that temperature is the primary factor for phase transformation, whereas the Zn plays a vital role in determining the c/a ratio of the HCP phase. The evaporation of Zn from the system causes a reduction in the *c*/*a* ratio of HCP phase, while turning high-entropy combination to medium-entropy combination. The evaporation of Zn even after forming part of the solid solution calls for caution regarding the design of HEAs using volatile elements such as Zn through mechanical alloying route, especially for high-temperature applications. Nevertheless, the stability and mechanical properties of AlCoTiZn HEA may be further enhanced by replacing Zn with another suitable element.


### Acknowledgments

This work is funded by the Science & Engineering Research Board, Department of Science & Technology (DST), India (No: EEQ/2017/000724). The authors are grateful to Dr. Suhash Ranjan Dey, Dr. Karre Rajamallu, Dr. Rahul Mane, Mr. Rameez Tamboli and Mr. Pritam Chakraborty for providing us support for DSC analysis in Materials Science and Metallurgical Engineering Department (IIT-Hyderabad) and support.


### Data Availability

The data are available on request.

### References


1. B. Cantor, Multicomponent and High Entropy Alloys, *Entropy*, 2014, **16**(9), p 4749–4768. https://doi.org/10.3390/e16094749
2. S. Thangaraju, T.E. Bouzy, and A. Hazotte, Phase Stability of a Mechanically Alloyed CoCrCuFeNi High Entropy Alloy, *Adv. Eng. Mater.*, 2017, **19**, p 1700095. https://doi.org/10.1002/adem.201700095
3. M. Detrois, S. Antonov, and S. Tin, Phase Stability and Thermodynamic Database Validation in a Set of Non-equiatomic Al-Co-Cr-Fe-Nb-Ni High-Entropy Alloys, *Intermetallics*, 2019, **104**, p 103–112. https://doi.org/10.1016/j.intermet.2018.11.002
4. R.B. Mane and B.B. Panigrahi, Comparative Study on Sintering Kinetics of As-Milled and Annealed CoCrFeNi High Entropy Alloy Powders, *Mater. Chem. Phys.*, 2018, **210**, p 49–56. https://doi.org/10.1016/j.matchemphys.2017.11.047
5. A. Sourav, S. Yebaji, and S. Thangaraju, Structure-Property Relationships in Hot Forged AlxCoCrFeNi High Entropy Alloys, *Mater. Sci. Eng. A.*, 2020, **793**, p 139877. https://doi.org/10.1016/j.msea.2020.139877
6. P. Chauhan, S. Yebaji, V.N. Nadakuduru, and T. Shanmugasundaram, Development of a Novel Light Weight Al35Cr14Mg6Ti35V10 High Entropy Alloy Using Mechanical Alloying and Spark Plasma Sintering, *J. Alloys Compd.*, 2020, **820**, p 153367. https://doi.org/10.1016/j.jallcom.2019.153367
7. A. Verma, P. Tarate, A.C. Abhyankar, M.R. Mohape, D.S. Gowtam, V.P. Deshmukh, and T. Shanmugasundaram, High Temperature Wear in CoCrFeNiCuxhigh Entropy Alloys: The Role of Cu, *Scr. Mater.*, 2019, **161**, p 28–31. https://doi.org/10.1016/j.scriptamat.2018.10.007
8. A.S. Negi, A. Sourav, M. Heilmaier, S. Biswas, and S. Thangaraju, Quantitative Phase Prediction in Dual-Phase High-Entropy Alloys: Computationally Aided Parametric Approach, *Phys. Status Solidi B.*, 2021, **258**, p 2100106. https://doi.org/10.1002/pssb.202100106
9. Y.H. Meng, F.H. Duan, J. Pan, and Y. Li, Phase Stability of B2-Ordered ZrTiHfCuNiFe High Entropy Alloy, *Intermetallics*, 2019, **111**, p 106515. https://doi.org/10.1016/j.intermet.2019.106515
10. J.Q. Yao, X.W. Liu, N. Gao, Q.H. Jiang, N. Li, G. Liu, W.B. Zhang, and Z.T. Fan, Phase Stability of a Ductile Single-Phase BCC Hf0.5Nb0.5Ta0.5Ti1.5Zr Refractory High-Entropy Alloy, *Intermetallics*, 2018, **98**, p 79–88. https://doi.org/10.1016/j.intermet.2018.04.023
11. R.B. Mane and B.B. Panigrahi, Effect of Alloying Order on Non-isothermal Sintering Kinetics of Mechanically Alloyed High Entropy Alloy Powders, *Mater. Lett.*, 2018, **217**, p 131–134. https://doi.org/10.1016/j.matlet.2018.01.092
12. T.-X. Li, J.-W. Miao, E.-Y. Guo, He. Huang, J. Wang, Lu. Yi-Ping, T.-M. Wang, Z.-Q. Cao, and T.-J. Li, Tungsten-Containing High-Entropy Alloys: A Focused Review of Manufacturing Routes, Phase Selection, Mechanical Properties, and Irradiation Resistance Properties, *Tungsten*, 2021, **3**, p 181–196. https://doi.org/10.1007/s42864-021-00115-4

13. T. Li, Y. Lu, Z. Cao, T. Wang, and T. Li, Opportunity and Challenge of Refractory High-Entropy Alloys in the Field of Reactor Structural Materials, *Acta Metall. Sin.*, 2021, **57**(1), p 42–54. https://doi.org/10.11900/0412.1961.2020.00293
14. T. Li, W. Jiao, J. Miao, Lu. Yiping, E. Guo, T. Wang, T. Li, and P.K. Liaw, A Novel ZrNbMoTaW Refractory High-Entropy Alloy with In-Situ Forming Heterogeneous Structure, *Mater. Sci. Eng. A*, 2021, **827**, p 142061. https://doi.org/10.1016/j.msea.2021.142061
15. T. Li, Lu. Yiping, T. Wang, and T. Li, Grouping Strategy via d-Orbit Energy Level to Design Eutectic High-Entropy Alloys, *Appl. Phys. Lett.*, 2021, **119**, p 071905. https://doi.org/10.1063/5.0061641
16. D.B. Miracle and O.N. Senkov, A Critical Review of High Entropy Alloys and Related Concepts, *Acta Mater.*, 2017, **122**, p 448–511. https://doi.org/10.1016/j.actamat.2016.08.081
17. Q. An, J. Wang, Y. Liu, B. Liu, W. Guo, Q. Fang, and Y. Nie, Effects of C and Mo on Microstructures and Mechanical Properties of Dual-Phase High Entropy Alloys, *Intermetallics*, 2019, **110**, p 106471. https://doi.org/10.1016/j.intermet.2019.04.014
18. M. Wang, H. Cui, Y. Zhao, C. Wang, N. Wei, X. Gao, and Q. Song, Enhanced Strength and Ductility in a Spark Plasma Sintered CoCrCu0.5NiAl0.5 High-Entropy Alloy via a Double-Step Ball Milling Approach for Processing Powders, *Mater. Sci. Eng. A.*, 2019, **763**, p 138071. https://doi.org/10.1016/j.msea.2019.138071
19. U. Häussermann and S.I. Simak, Origin of the (Formula Presented) Variation in Hexagonal Close-Packed Divalent Metals, *Phys. Rev. B Condens. Matter Mater. Phys.*, 2001, **64**, p 1–10. https://doi.org/10.1103/PhysRevB.64.245114
20. M.C. Gao, B. Zhang, S.M. Guo, J.W. Qiao, and J.A. Hawk, High-Entropy Alloys in Hexagonal Close-Packed Structure, *Metall. Mater. Trans. A Phys. Metall. Mater. Sci.*, 2016, **47**, p 3322–3332. https://doi.org/10.1007/s11661-015-3091-1
21. A. Ter-Isahakyan, J.S. Rau, and T.J. Balk, High Entropy Alloys with Hexagonal Close-Packed Structure Derived from Thin Film Combinatorial Approach, *J. Alloys Compd.*, 2022, **893**, p 162293. https://doi.org/10.1016/j.jallcom.2021.162293
22. X.-T. Chen, L. Shao, T.-W. Fan, J.-M. Duan, and B.-Y. Tang, Investigation of Aluminum Concentration on Stacking Fault Energies of Hexagonal Close-Packed High-Entropy Alloys, Hf0.25Ti0.25Zr0.25Sc0.25−xAlx (x < 15%), *J. Alloys Compd.*, 2021, **887**, p 161412. https://doi.org/10.1016/j.jallcom.2021.161412
23. X. Yang and Y. Zhang, Prediction of High-Entropy Stabilized Solid-Solution in Multi-Component Alloys, *Mater. Chem. Phys.*, 2012, **132**, p 233–238. https://doi.org/10.1016/j.matchemphys.2011.11.021
24. S. Varalakshmi, M. Kamaraj, and B.S. Murty, Synthesis and Characterization of Nanocrystalline AlFeTiCrZnCu High Entropy Solid Solution by Mechanical Alloying, *J Alloys Compd.*, 2008, **460**, p 253–257. https://doi.org/10.1016/j.jallcom.2007.05.104
25. S. Varalakshmi, G. Appa Rao, M. Kamaraj, and B.S. Murty, Hot Consolidation and Mechanical Properties of Nanocrystalline Equiatomic AlFeTiCrZnCu High Entropy Alloy After Mechanical Alloying, *J. Mater. Sci.*, 2010, **45**, p 5158–5163. https://doi.org/10.1007/s10853-010-4246-5
26. S. Varalakshmi, M. Kamaraj, and B.S. Murty, Processing and Properties of Nanocrystalline CuNiCoZnAlTi High Entropy Alloys by Mechanical Alloying, *Mater. Sci. Eng. A*, 2010, **527**, p 1027–1030. https://doi.org/10.1016/j.msea.2009.09.019
27. K.G. Pradeep, N. Wanderka, P. Choi, J. Banhart, B.S. Murty, and D. Raabe, Atomicscale Compositional Characterization of a Nanocrystalline AlCrCuFeNiZn High-Entropy Alloy Using Atom Probe Tomography, *Acta Mater.*, 2013, **61**, p 4696–4706. https://doi.org/10.1016/j.actamat.2013.04.059
28. F. Salemi, M.H. Abbasi, and F. Karimzadeh, Synthesis and Thermodynamic Analysis of Nanostructured CuNiCoZnAl High Entropy Alloy Produced by Mechanical Alloying, *J Alloys Compd.*, 2016, **685**, p 278–286. https://doi.org/10.1016/j.jallcom.2016.05.274
29. S. Varalakshmi, M. Kamaraj, and B.S. Murty, Formation and Stability of Equiatomic and Nonequiatomic Nanocrystalline CuNiCoZnAlTi High-Entropy Alloys by Mechanical Alloying, *Metall. Mater. Trans. A*, 2010, **41**, p 2703–2709. https://doi.org/10.1007/s11661-010-0344-x
30. S. Mohanty, N.P. Gurao, and K. Biswas, Sinter Ageing of Equiatomic Al20Co20Cu20Zn20Ni20 High Entropy Alloy via Mechanical Alloying, *Mater. Sci. Eng A*, 2014, **617**, p 211–218. https://doi.org/10.1016/j.msea.2014.08.046
31. K.R. Cardoso, B. da Silva Izaias, L. de Souza Vieira, and A.M. Bepe, Mechanical Alloying and Spark Plasma Sintering of AlCrCuFeZn High Entropy Alloy, *Mater. Sci. Technol.*, 2020, **36**(17), p 1861–1869. https://doi.org/10.1080/02670836.2020.1839195
32. S. Mridha, S. Samal, P. Yousaf Khan, K. Biswas, and A. Govind, Processing and Consolidation of Nanocrystalline Cu-Zn-Ti-Fe-Cr High-Entropy Alloys via Mechanical Alloying, *Metall. Mater. Trans. A*, 2013, **44**, p 4532–4541. https://doi.org/10.1007/s11661-013-1824-6
33. Y.-L. Chen, C.-W. Tsai, C.-C. Juan, M.-H. Chuang, J.-W. Yeh, T.-S. Chin, and S.-K. Chen, Amorphization of Equimolar Alloys with HCP Elements During Mechanical Alloying, *J. Alloys Compd.*, 2010, **506**, p 210–215. https://doi.org/10.1016/j.jallcom.2010.06.179
34. Y. Zhang, T.T. Zuo, Z. Tang, M.C. Gao, K.A. Dahmen, P.K. Liaw, and Z.P. Lu, Microstructures and Properties of High-Entropy Alloys, *Prog. Mater. Sci.*, 2014, **61**, p 1–93. https://doi.org/10.1016/j.pmatsci.2013.10.001
35. M. Feuerbacher, M. Heidelmann, and C. Thomas, Hexagonal High-Entropy Alloys, *Mater. Res. Lett.*, 2015, **3**(1), p 1–6. https://doi.org/10.1080/21663831.2014.951493
36. K.M. Youssef, A.J. Zaddach, C. Niu, D.L. Irving and C.C. Koch, A Novel Low-Density, High-Hardness, High- entropy Alloy with Close-Packed Single-Phase Nanocrystalline Structures, *Mater. Res. Lett.*, 2015, **3**(2), p 95–99. https://doi.org/10.1080/21663831.2014.985855
37. S. Guo, C. Ng, J. Lu, and C.T. Liu, Effect of Valence Electron Concentration on Stability of fcc or bcc Phase in High Entropy Alloys, *J. Appl. Phys.*, 2011, **109**, p 103505. https://doi.org/10.1063/1.3587228
38. C.Y. Cheng, Y.C. Yang, Y.Z. Zhong, Y.Y. Chen, T. Hsu, and J.W. Yeh, Physical Metallurgy of Concentrated Solid Solutions from Low-Entropy to High-Entropy Alloys, *Curr. Opin. Solid State Mater. Sci.*, 2017, **21**, p 299–311. https://doi.org/10.1016/j.cossms.2017.09.002
39. P. Chauhan, S. Chopra, and S. Thangaraju, Inter-Dependency Relationships in High-Entropy Alloys: Phase Stability Criteria, *Adv. Eng. Mater.*, 2019, **21**, p 1900251. https://doi.org/10.1002/adem.201900251
40. Weights and Atomic Numbers of the elements, General Physical and Chemical Constants, in *Smithells Metals Reference Book*, 2003, p 1–11. https://doi.org/10.1016/B978-075067509-3/50006-3
41. É. Fazakas, V. Zadorozhnyy, and D.V. Louzguine-Luzgin, Effect of Iron Content on the Structure and Mechanical Properties of Al 25 Ti 25 Ni 25 Cu 25 and (AlTi) 60-x Ni 20 Cu 20 Fe x (x=15, 20) high-Entropy Alloys, *Appl. Surf. Sci.*, 2015, **358**, p 549–555. https://doi.org/10.1016/j.apsusc.2015.07.207
42. S.G. Ma and Y. Zhang, Effect of Nb Addition on the Microstructure and Properties of AlCoCrFeNi High-Entropy Alloy, *Mater. Sci. Eng. A.*, 2012, **532**, p 480–486. https://doi.org/10.1016/j.msea.2011.10.110
43. C. Li, J.C. Li, M. Zhao, and Q. Jiang, Effect of Alloying Elements on Microstructure and Properties of Multiprincipal Elements High-Entropy Alloys, *J. Alloys Compd.*, 2009, **475**, p 752–757. https://doi.org/10.1016/j.jallcom.2008.07.124
44. O.N. Senkov, S.V. Senkova, D.B. Miracle, and C. Woodward, Mechanical Properties of Low-Density, Refractory Multi-principal Element Alloys of the Cr-Nb-Ti-V-Zr System, *Mater. Sci. Eng. A.*, 2013, **565**, p 51–62. https://doi.org/10.1016/j.msea.2012.12.018
45. Y.X. Zhuang, W.J. Liu, Z.Y. Chen, H.D. Xue, and J.C. He, Effect of Elemental Interaction on Microstructure and Mechanical Properties of FeCoNiCuAl Alloys, *Mater. Sci. Eng. A.*, 2012, **556**, p 395–399. https://doi.org/10.1016/j.msea.2012.07.003